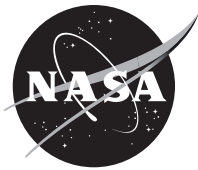# Vacuum Melt Infiltration of 2D Tyranno SA3® Ceramic Matrix Composites With Cr-25(wt.%)Si Intermetallic Alloy

S.V. Raj
Glenn Research Center, Cleveland, Ohio

NASA STI Program . . . in Profile

Since its founding, NASA has been dedicated to the advancement of aeronautics and space science. The NASA Scientific and Technical Information (STI) Program plays a key part in helping NASA maintain this important role.

The NASA STI Program operates under the auspices of the Agency Chief Information Officer. It collects, organizes, provides for archiving, and disseminates NASA's STI. The NASA STI Program provides access to the NASA Technical Report Server—Registered (NTRS Reg) and NASA Technical Report Server—Public (NTRS) thus providing one of the largest collections of aeronautical and space science STI in the world. Results are published in both non-NASA channels and by NASA in the NASA STI Report Series, which includes the following report types:

- TECHNICAL PUBLICATION. Reports of completed research or a major significant phase of research that present the results of NASA programs and include extensive data or theoretical analysis. Includes compilations of significant scientific and technical data and information deemed to be of continuing reference value. NASA counter-part of peer-reviewed formal professional papers, but has less stringent limitations on manuscript length and extent of graphic presentations.

- TECHNICAL MEMORANDUM. Scientific and technical findings that are preliminary or of specialized interest, e.g., "quick-release" reports, working papers, and bibliographies that contain minimal annotation. Does not contain extensive analysis.

- CONTRACTOR REPORT. Scientific and technical findings by NASA-sponsored contractors and grantees.

- CONFERENCE PUBLICATION. Collected papers from scientific and technical conferences, symposia, seminars, or other meetings sponsored or co-sponsored by NASA.

- SPECIAL PUBLICATION. Scientific, technical, or historical information from NASA programs, projects, and missions, often concerned with subjects having substantial public interest.

- TECHNICAL TRANSLATION. English-language translations of foreign scientific and technical material pertinent to NASA's mission.

For more information about the NASA STI program, see the following:

- Access the NASA STI program home page at http://www.sti.nasa.gov

- E-mail your question to help@sti.nasa.gov

- Fax your question to the NASA STI Information Desk at 757-864-6500

- Telephone the NASA STI Information Desk at 757-864-9658

- Write to:
  NASA STI Program
  Mail Stop 148
  NASA Langley Research Center
  Hampton, VA 23681-2199

NASA/TM-20220006118

Vacuum Melt Infiltration of 2D Tyranno SA3® Ceramic Matrix Composites With Cr-25(wt.%)Si Intermetallic Alloy

S.V. Raj
Glenn Research Center, Cleveland, Ohio

September 2022

Acknowledgments

Level of Review: This material has been technically reviewed by technical management.

Vacuum Melt Infiltration of 2D Tyranno SA3® Ceramic Matrix Composites With Cr-25(wt.%)Si Intermetallic Alloy

S.V. Raj
National Aeronautics and Space Administration
Glenn Research Center
Cleveland, Ohio 44135

Abstract

The potential and limitations of vacuum melt infiltrating woven preforms of 2D Tyranno SA3 fibers with Cr-25(wt.%)Si alloy were investigated. Microstructural observations revealed that the volume fractions of open voids infiltrated by the molten metal varied between 3.7 and 10.0% irrespective of the magnitudes of the melt infiltration temperatures and hold times, which was attributed in part to substantial volatilization of the silicide charge based on computational thermodynamics. In the absence of experimental data, poor wettability of the melt could not be ruled out unambiguously. Other possible reasons are carefully examined and discarded. Ring microstructures were observed around the fibers mainly at the outer surfaces of the infiltrated preform, where the BN and chemical vapor infiltrated SiC coatings had vaporized in the high vacuum environment. In contrast, they were absent in the interior of the preform, where the coatings were still present with no evidence of molten metal attack of the coatings. Details of thermodynamic calculations are presented to confirm the volatilization of the BN and CVI SiC coatings thereby resulting in the ring microstructures due to the filling of voids by the molten silicide. It is concluded that successful melt infiltration of Tyranno SA3®[1] with Cr-25%Si can be only achieved under sufficient positive pressure to prevent volatilization of the coatings and the molten silicide.

1.0 Introduction

Silicon carbide fiber-reinforced ceramic matrix composites (CMCs) are being developed for jet-fueled aircraft engine applications over the last several decades [1-14]. Thus, hot section components, such as combustor liners, shrouds, and turbine blades and vanes, made of the lightweight SiC_f/SiC_m[2] CMCs can operate at higher temperatures and higher pressure ratios with reduced cooling air resulting in increased engine efficiency, lower fuel burn thereby leading to lower CO_2 emissions, and significant cost savings in the operation of each aircraft.

However, the low toughness of the SiC_m matrix CMCs limits their design stresses to typically less than the tensile proportional stress of the CMC due to the relatively low matrix cracking stress of less than 192 MPa [9,15-18]. Environmental factors, such as oxygen ingress through surface-connected cracks can react with the BN coatings on the fibers to form low melting borosilicate glass and critically limit CMC life [9] and/or moisture attack of the fibers and the matrix, can also lessen CMC durability. Additionally, the presence of unconverted residual silicon (i.e., "free silicon") in SiC_m/SiC_f CMCs fabricated by silicon melt infiltration (MI) significantly limits its use temperature to well below the melting point of Si to ensure that the CMC component has acceptable creep and thermomechanical properties. As a result, conventional silicon MI techniques cannot be used for fabricating SiC_m/SiC_f CMCs for applications typically above 1588 K (2400 °F) and as high as 1755 K (2700 °F).

---

[1] Trademark of Ube Industries, Ltd., Tokyo, Japan.
[2] In this paper, SiC_f specifically refers to long fibers in CMCs in contrast to SiC_P particulates and SiC_W whiskers used in particulate and whisker-reinforced composites, respectively.

Thus, it is important to investigate whether metallic systems with melting points higher than silicon can be used to infiltrate SiC_f preforms for applications as high as 1755 K. Compared to silicon MI of woven SiC_f preforms [6-8,19], the literature on silicide MI of these preforms is sparse. Since the thermal expansions of several common silicides are significantly higher than those of SiC_f [20], it is important to minimize the resulting differences in thermal strain between SiC_f and the silicide matrix for high temperature applications. Thus, a generalized theoretical model was proposed for designing engineered matrices (EM) to minimize the thermal strains between the fibers and the EM., which was verified in detailed proof-of-concept studies [20]. It was demonstrated that two EMs consisting of 10(vol.%)$CrSi_2$-70%SiC-20%Si_3N_4 ($CrSi_2$-EM) and 10(vol.%)CrMoSi-60%SiC-30%Si_3N_4 (CrMoSi-EM), where CrMoSi is an abbreviation for the Cr-30(at.%) Mo-30%Si alloy [21-25], possessed the best combination of bend ductility, bend strength and oxidation properties [26]. The CrMoSi-EM matrix is of particular interest as a high temperature silicide matrix for applications up to 1750 K due to the high absolute melting temperature, T_m, of CrMoSi [22,23].

The proposed method for fabricating high temperature engineered ceramic matrix composites (E-CMCs) with a CrMoSi-EM containing self-healing additives is described elsewhere [27]. It is envisioned that the CrMoSi-EM would be first slurry infiltrated into SiC_f woven preform specimens to fill in as much of the open voids as possible. Next, the preform would be melt-infiltrated with either molten $CrSi_2$ or a nominal Cr-25(wt.%)Si[3] to fill in the gaps in the slurry-infiltrated preform with relatively small amounts of the molten silicide so as to bind the CrMoSi-EM powder particles as binding agent. The final step would consist of a suitable post-MI heat treatment of the E-CMC to ensure that the MI $CrSi_2$ or the Cr-25%Si alloy diffuses into the CrMoSi particles to prevent incipient melting above 1760 K and to ensure adequate creep strength of the matrix at and below 1750 K.

The larger objectives of the present investigation were to study the temperature conditions for vacuum melt infiltrating (VMI) woven Tyranno SA3 preform specimens with molten $CrSi_2$ and nominal Cr-25%Si. An earlier paper examined the processing parameters for VMI of Tyranno SA3 preforms with $CrSi_2$ and concluded that substantial volatilization of $CrSi_2$ decreased the amount of infiltration at higher absolute MI temperatures, T_{MI} [27]. The present paper reports the results of a parallel study conducted to establish the processing conditions for VMI of Tyranno SA3 with molten Cr-25%Si[4]. There appears to be no prior literature on this topic.

The Cr-25%Si alloy corresponds to a single phase region of the Cr-Si binary phase diagram with the room temperature phase being α-Cr_5Si_3, which transforms to the high temperature β-Cr_5Si_3 phase at about 1778 K (Figure 1) [28]. The approximate values of the absolute solidus, T_S, and liquidus, T_L, temperatures for the Cr-25%Si alloy are about 1778 K and 1953 K, respectively. As shown in Figure 1, there is uncertainty in the exact magnitudes of these values of T_S and T_L. In contrast, the CrSi phase is a line compound with T_m =1686 K, which is significantly less than that for $CrSi_2$ (T_m = 1763 K). In addition, CrSi, as well as any eutectic two phase CrSi+ α-Cr_5Si_3 matrix composition, would melt at 1686 K thereby limiting the E-CMC application temperature to less than 1686 K if residual CrSi is present in the matrix. Thus, the higher liquidus and solidus temperatures for the Cr-25%Si alloy pose a distinct advantage over both CrSi and $CrSi_2$ for the desired application temperatures. However, MI above 1880 K corresponding to the (L + β-Cr_5Si_3) region, where L stands for "liquid", could lead to detrimental microstructural changes in the fibers and coatings, the possibility of molten metal reaction, and fiber fusion. The present paper also examines the chemical compatibility of Cr-25%Si with the SiC fibers, the BN coating, or the chemical vapor infiltrated (CVI) SiC coating.

---

[3] Unless otherwise indicated, all compositions are reported in wt.% in this paper. The nominal composition Cr-25(wt.%)Si corresponds to Cr-38.2(at.%)Si.

[4] It is important to note that these preforms do not contain the engineered matrices to compensate for the thermal expansion differences between Cr-25%Si and Tyranno SA3 fibers as would be required in fabricating E-CMCs.

Atomic percent silicon

0   10   20   30   40   50   60   70   80   90   100

2000

1863 °C

1800

1770 °C

9

22

5.4 1705 °C   1660   1680 °C

(Cr)   13.6   23

βCr₅Si₃

1600

1505 °C

1490 °C

Cr₃Si

1413 °C 36

1414 °C

1400   27   35   1390 °C

41   51.93

1305 °C

52.29   71

1×10⁻⁵ wt% Cr

1200

αCr₅Si₃

CrSi

CrSi₂

1000

(Si)→

800

0   10   20   30   40   50   60   70   80   90   100
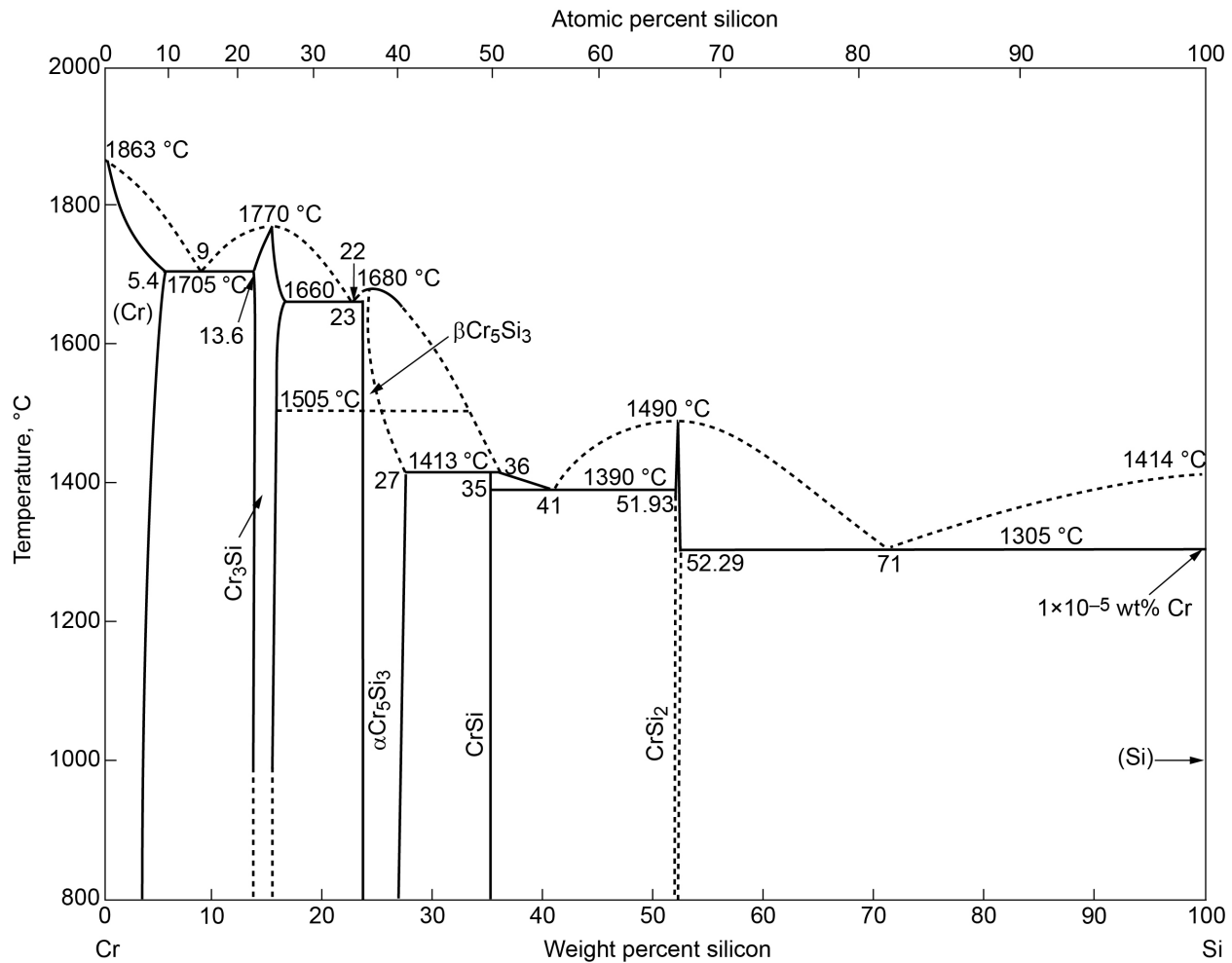
Cr   Weight percent silicon   Si

Figure 1.—Cr-Si binary phase diagram [28]. (Reprinted with permission of ASM International. All rights reserved).

2.0 Experimental Procedures

The materials and experimental procedures used in this investigation were similar to those employed for melt infiltrating Tyranno SA3 preforms with molten $CrSi_2$ [27]. Therefore, only a brief description is provided in this paper. The dimensions of the specimens used for the VMI studies were 10 x 10 x 2.1 mm, which were diamond saw cut from a larger panel 235 x 160 x 2.1 mm (6-ply) at low cutting speeds to minimize fiber damage. The measured average volume fraction of the open porosity, V_0, was determined to be $23.8 \pm 0.3\%$[5] based on geometrical and immersion density measurements on four specimens machined from the panel [27].

Two Cr-25%Si alloy buttons each weighing about 25 g were prepared by arc melting high purity Cr and Si chunks, which were weighed in the appropriate amounts and mixed together to obtain the desired nominal composition. Each button was separately fabricated by melting the charge in an arc melting furnace. The melt was flipped several times to ensure that the Cr and Si had completely reacted before casting the molten metal into a water-cooled copper mold to form the button. The buttons were broken into small pieces and further crushed into powder using a mortar and pestle for use in MI. The buttons

---

[5] It is noted that unless otherwise mentioned that the error limits shown in this paper refer to the 95% confidence limits.

were not homogenized annealed prior to crushing into powder since the composition would homogenize during heating to T_{MI}.

A small amount of powder was submitted for x-ray diffraction (XRD) analyses to determine the phases present in the arc-melted alloy powders using Cu K_α radiation. Although quantitative phase analysis (QPA) was conducted on the XRD spectrum using a full pattern fitting software, the results may not be completely reliable due to poor sampling statistics. Thus, the QPA results reported in this present paper must be accepted with some degree of caution. The chemical analyses of the powders obtained were determined by the induction coupled plasma (ICP) technique. The amounts of N and O were determined by NSL Analytical Services, Cleveland, Ohio. X-ray fluorescence (XRF) was used to assess the Cr and Si amounts in a chunk of the alloy.

2.1 Melt Infiltration

Vacuum MI of the Tyranno SA3 preforms was conducted in a high vacuum graphite melt furnace. Details of the set-up are described elsewhere [27]. The weight of the Cr_5Si_3 powder, $(W_{CS})_{exp}$, varied between 2.2 and 12.5 g. Most of the MI trials were conducted without an external weight. However, in a few instances placing an external graphite or SiC weight with its bottom painted with BN paste on top of the silicide powder did not increase the amount of silicide infiltration into the preform. The SiC weight varied between 13.2 and 102 g. A carbon matte and the preform were weighed separately. The carbon matte was placed on a BN-painted or sprayed graphite plate and the preform was placed on top of it. The Cr_5Si_3 powder was sprinkled on top of the preform and all around it. The BN-coated graphite plate and its contents were introduced into the furnace, which was evacuated to vacuum levels between 1.3×10^{-2} and 6.7×10^{-4} Pa (10^{-4} and 5×10^{-6} torr) before heating the furnace at 600 K/h to T_{MI}. The magnitudes of T_{MI} varied between 1823 and 1958 K for hold times, t_{MI}, varying between 1800 and 3600 s. As noted earlier, it was important to ensure that $T_S < T_{MI} < T_L$ to minimize potential fiber damage and reaction with the molten silicide. Thus, with the exception of the specimen infiltrated at 1958 K, there was always some unmelted residual material left on top and at the sides of the preform so that the actual amount of material that infiltrated the preform was less than the original weighed charge. The specimens were furnace cooled to room temperature under vacuum after MI.

2.2 Characterization

X-ray micro-computed tomography (μ-CT) were performed on a 10 x 10 mm preform specimen to obtain a large number of cross-sectional images spaced 10 μm apart, which were stitched together by the instrument's software to reveal the void morphology in the uninfiltrated preform. Transverse cross-sections cut from the MI specimens were mounted and polished for metallographic observations. The specimens were characterized using optical microscopy (OM), scanning electron microscopy (SEM), back scattered electron (BSE) imaging and energy dispersive spectroscopy (EDS). Several low magnification digital OM images of the cross-sections of the MI samples were obtained at 25x for volume fraction measurements. Focused Ion Beam (FIB) was used for precisely milling sections of a polished MI specimen to study the microstructure along the fiber direction. In this case, the specimen was sputter-coated with platinum (Pt) prior to milling.

The volume fraction measurements were made by separately counting the number of grid points that lay either on silicide-filled open voids or on the unfilled voids and dividing each by the total number of grid points using a grid size of 20 x 20 mm in Adobe Photoshop CS6[6]. The number of images used for

---

[6] Trademark of Adobe Systems, Inc.

making these measurements varied between 3 and 6 per MI preform with the total number of grid points selected varying between about 115 and 276. The average volume fractions of the silicide-filled open voids, V_I, and unfilled voids, V_U, for each specimen, and the corresponding 95% confidence error bars are reported in this paper[7]. It is important to note that V_U includes both the unfilled open and closed intra- and inter-tow voids while V_I represents only the volume fraction of open voids in the intra- and inter-tow regions that were infiltrated by the melt.

3.0   Results and Discussion

3.1   Characteristics of the Starting Materials

Table I shows the actual compositions of Cr-25%Si powder determined by ICP as well as XRF. The ICP results suggested that the silicon content was about 22% while the XRF data of about 24% was closer to the nominal composition of 25%. The difference in the two experimental values were within 2.5%. This discrepancy could be due to uncertainties in the XRF readings, spatial compositional inhomogeneity in the as-cast buttons and because not all the silicon in the alloy dissolved in the solvent prior to the ICP analysis thereby resulting in a lower silicon reading. Therefore, the alloy will be referred by its nominal composition Cr-25%Si in this paper.

The μ-CT scanned image showed that the 0° and 90° fiber tows were tightly woven with the voids distributed between them (Figure 2(a)). Figure 2(b) shows the optical microstructure of a cross-section of a different Tyranno SA3 preform, where it is evident that the porosity is distributed as intra- and inter-tow voids [27]. It is important to note that many of the voids could be surface-connected at other out-of-plane sections within the preform.

3.2   Optical Microstructures of the Melt-Infiltrated Preforms

The measured equilibrium contact angles for wetting, θ_e, for Cr_5Si_3[8] alloy and silicon on SiC are less than 40° [29]. It has been demonstrated that $\theta_e < 90°$ for molten $CrSi_2$ on a SiC substrate with good wettability [30]. It is important to note that the magnitude of θ_e will be influenced by the presence of a SiO_2 layer on the SiC_f tows with values of $\theta_e \sim 90°$ for Si on SiO_2 [31]. In non-reactive molten metal-ceramic substrate systems, good wettability is attained when $0° < \theta_e < 90°$ with typical values of $\theta_e \sim 40$-$50°$ for molten Si on a SiC substrate [31-33]. Similarly, it is expected that the Cr-25%Si alloy should exhibit good wettability with the Tyranno SA3 preforms during MI. Although the magnitude of θ_e is assumed commonly to be a measure of wettability, Warren and Anderson [34] have cautioned that a better measure of wettability is the product $\gamma_{SV} \cos \theta_e$, where γ_{SV} is the specific surface energy of the molten drop with the atmosphere since a low value of γ_{SV} can result in poor wettability even when $0° < \theta_e < 90°$.

---

[7] As noted later in the paper, the microstructures at some locations close to the outer surfaces of the MI preforms showed ring microstructures unlike those in the interior. The values of V_I and V_U reported in this paper represent regions where the microstructures were uniform without any ring microstructures.

[8] Champion et al. [29] identified the phase as Cr_3Si_2 in their paper instead of Cr_5Si_3, which is the phase identified in the binary Cr-Si phase diagram (Figure 1) [28]. Since the Cr:Si ratio for Cr_3Si_2 is 1.5, it is suggested that the phase referred to in Ref. [29] was misidentified and actually refers to the Cr_5Si_3 phase in the phase diagram for which Cr:Si is about 1.67.

TABLE I.—CHEMICAL COMPOSITION OF THE Cr-25%Si POWDER IN wt.%

Method	Cr	Si	C	O	Ti
ICP, wt.%	78.0	21.8	0.02	0.43	< 0.001
XRF, wt.%	75.5	24.2	-----	-----	---------

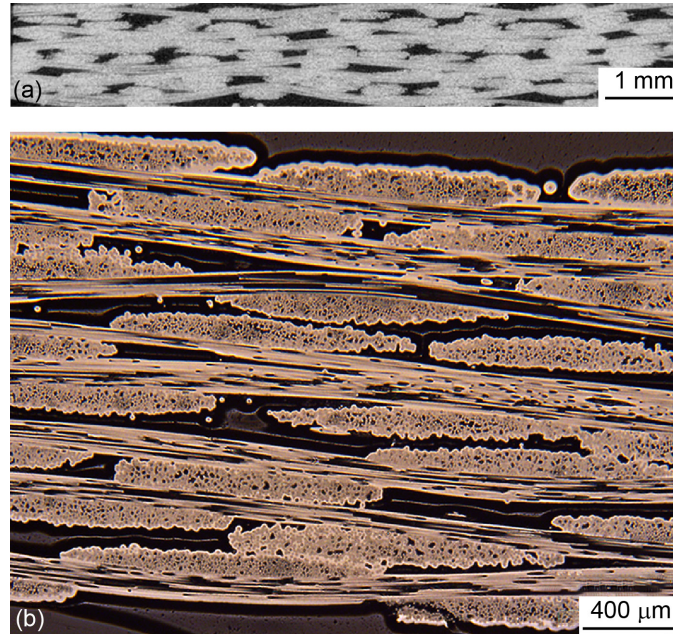

Figure 2.—(a) μ–CT image and (b) optical microstructure of the cross-section of an as-received Tyranno SA3 preform [27]. The μ–CT and the optical images were obtained from different specimens.

Table II tabulates the values of V_I and V_U for different values of T_{MI} and t_{MI}. The magnitudes of V_I and V_U range between 3.7 and 11.9%, and 13.7 and 35.5%, respectively. Figure 3 shows an overview of a specimen infiltrated at 1823 K for a hold time of 3600 s. It is clear that the preform is only partially filled with the molten metal with $V_I = 6.9 \pm 3.1\%$. A significant amount of the melt had solidified at the outer surfaces without infiltrating the preform. Similarly, a specimen infiltrated at 1843 K for 1800 s showed relatively little infiltration with $V_I = 4.1 \pm 2.7\%$ (Figure 4). These observations suggest that wettability was lower than expected. Once again, there was relatively low infiltration of the melt with most of it solidifying on the outer surfaces. The fact that T_{MI} was 20 K higher than that for the specimen infiltrated at 1823 K (Figure 3) suggested that an increase in the fluidity of the melt was insufficient to make a difference. Similarly, increasing T_{MI} to higher temperatures from 1873 to as high as 1958 K above T_L did not increase the amount of infiltration (Figure 5 to Figure 8). Clearly, increasing the fluidity of the molten metal with increasing temperature did not increase V_I. It was reported in an earlier paper on the MI of Tyranno SA3 preforms with $CrSi_2$ [27] that V_I was independent of t_{MI} in an earlier investigation. A similar trend was observed in the present study (Table II). These observations indicate that MI occurred in a relatively short period of time much less than the experimental t_{MI}.

TABLE II.—AVERAGE VOLUME FRACTIONS OF THE SILICIDE-FILLED
OPEN VOIDS, V_I, AND UNFILLED VOIDS, V_U, WITH THE
CORRESPONDING 95% CONFIDENCE VALUES FOR
DIFFERENT MI TEMPERATURES AND TIMES

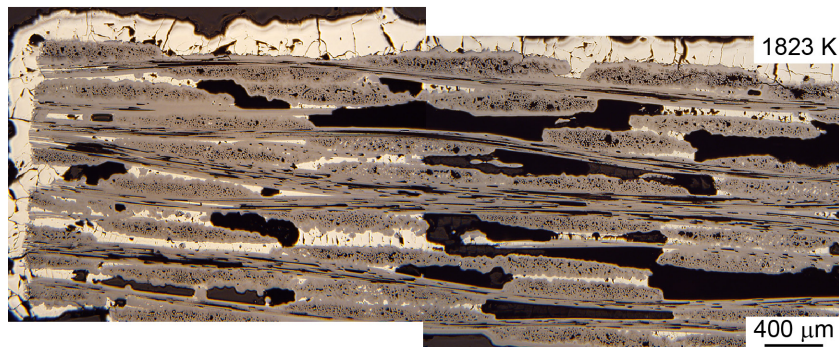| T_{MI} (K)	t_{MI} (s)	V_I (%)	V_U (%)
1823	3600	6.9 ± 3.1	26.3 ± 11.0
1843	1800	4.1 ± 2.7	25.3 ± 6.2
1853*	3600	3.7 ± 2.1	35.5 ± 10.1
1853	3600	6.3 ± 4.8	33.6 ± 6.6
1858	1800	5.9 ± 1.8	27.8 ± 7.3
1873	1800	10.0 ± 1.7	13.7 ± 6.0
1873	3600	8.6 ± 4.0	16.4 ± 4.6
1883	3600	5.1 ± 1.9	18.1 ± 0.9
1900	3600	11.9 ± 4.0	25.5 ± 7.3
1923	3600	6.6 ± 2.0	20.4 ± 0.5
1958	3600	3.7 ± 1.0	31.3 ± 3.0

*Pre-oxidized.

Figure 3.—Composite optical micrograph of a preform melt-infiltrated with Cr-25%Si at 1823 K for 3600 s showing incomplete infiltration of the voids with $V_I = 6.9 \pm 3.1\%$. A large amount of the solidified alloy is observed at the outer surfaces of the preform.

A careful examination of Figure 3 to Figure 8 revealed several general observations. First, a significant amount of solidified alloy was observed on the outer surfaces of the preforms for $T_{MI} < 1873$ K while being largely absent when $T_{MI} \geq 1873$ K. Second, the morphology of the meniscus of the solidified alloy within the pores of the preform often showed that approximately $60° < \theta_e < 90°$ while in other instances it was perpendicular to the orientation of the fibers with $\theta_e \approx 90°$. While the temperature dependence of θ_e for the Cr-25%Si/Tyranno SA3 system is unknown, and these qualitative observations suggest that the alloy may possess good wettability characteristics consistent with literature data [29], it is cautioned that a low value of γ_{SV} could result in poor wettability even when $0° < \theta_e < 90°$ [34]. Thus, the effect of wettability in influencing the extent of infiltration in the present study is unclear at this time. Third, the preforms appeared to have deformed and shrunk in size when $T_{MI} > 1873$ K with the fibers showing clear evidence of fusion at $T_{MI} = 1958$ K (Figure 9). Fourth, single and double ring microstructures were observed in some areas

primarily near the outer surfaces, where the molten metal had solidified in either one or two rings around the fibers, respectively (Figure 10(a)). In these instances, the molten metal had also infiltrated along the columnar grain boundaries of the CVI SiC coating. This microstructure was not commonly observed in the interior (Figure 10(b)). These microstructural observations are discussed in greater detail in Section 3.5.
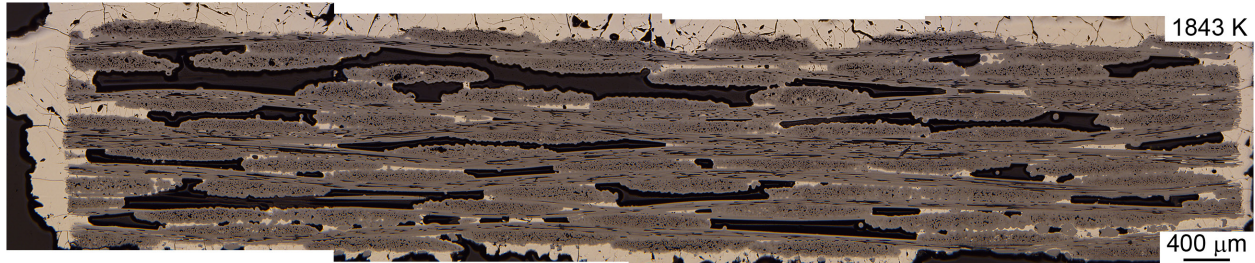

Figure 4.—Composite optical micrograph of a preform melt-infiltrated with Cr-25%Si at 1843 K for 1800 s showing incomplete infiltration of the voids with V_I = 4.1 ± 2.7%. A large amount of the solidified alloy is observed at the outer surfaces of the preform.
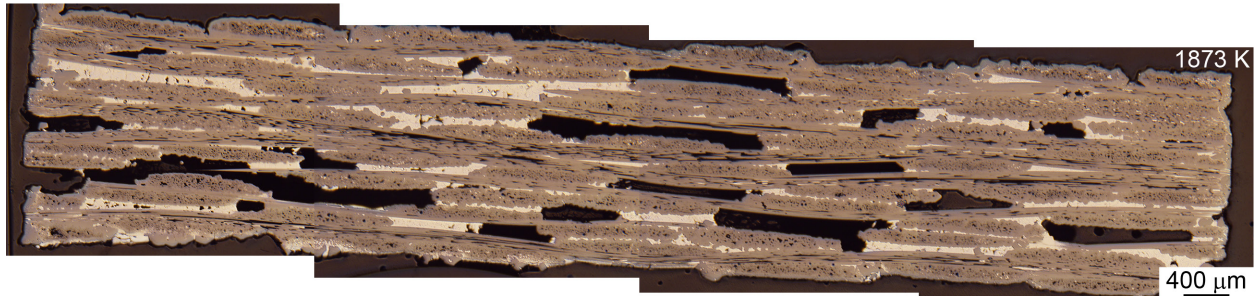

Figure 5.—Composite optical micrograph of a preform melt-infiltrated with Cr-25%Si at 1873 K for 3600 s showing incomplete infiltration of the voids with V_I = 8.6 ± 4.0%. No solidified alloy is observed at the outer surfaces of the preform.

Figure 6.—Composite optical micrograph of a preform melt-infiltrated with Cr-25%Si at 1900 K for 3600 s showing incomplete infiltration of the voids with V_I = 11.9 ± 4.0%. The preform appears to have shrunk and deformed. No solidified alloy is observed at the outer surfaces of the preform.
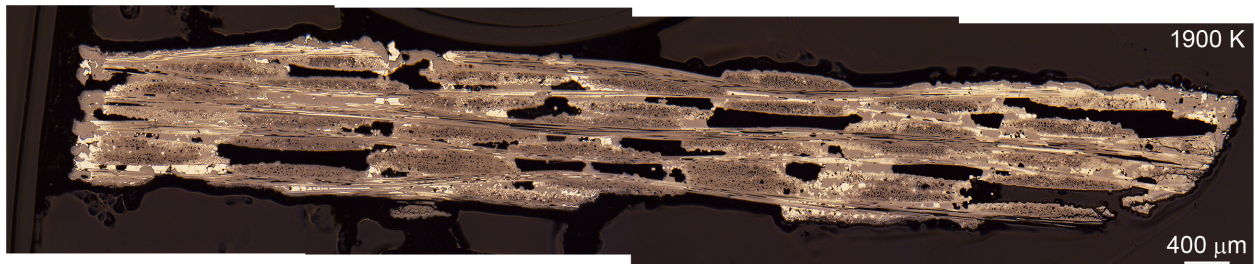
Figure 7.—Composite optical micrograph of a preform melt-infiltrated with Cr-25%Si at 1923 K for 3600 s showing incomplete infiltration of the voids with V_I = 6.6 ± 2.0%. Some solidified alloy is observed at the outer surfaces of the preform.
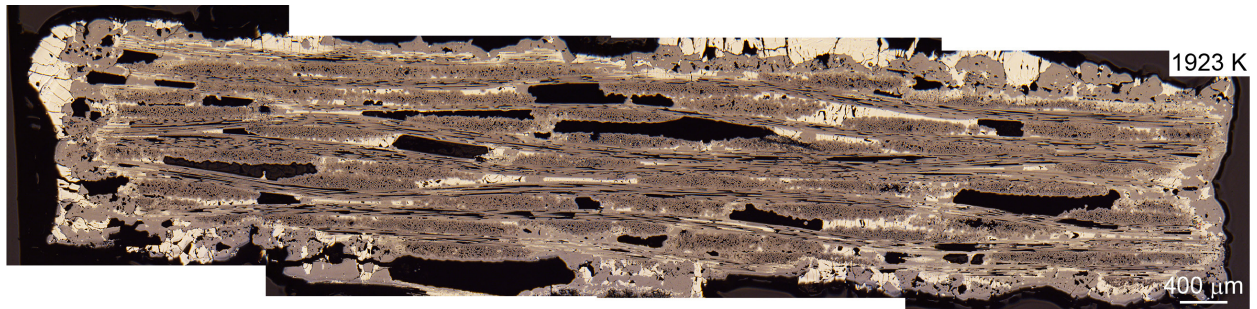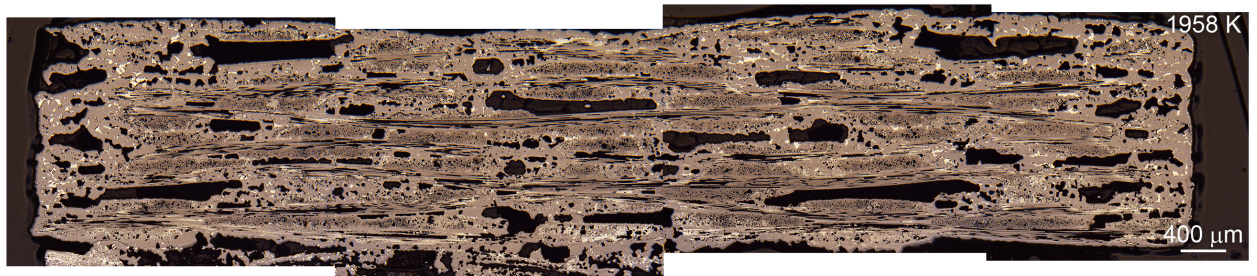

Figure 8.—Composite optical micrograph of a preform melt-infiltrated with Cr-25%Si at 1958 K for 3600 s showing incomplete infiltration of the voids with V_I = 3.7 ± 1.0%. The preform appears to have shrunk and deformed. No solidified alloy is observed at the outer surfaces of the preform.
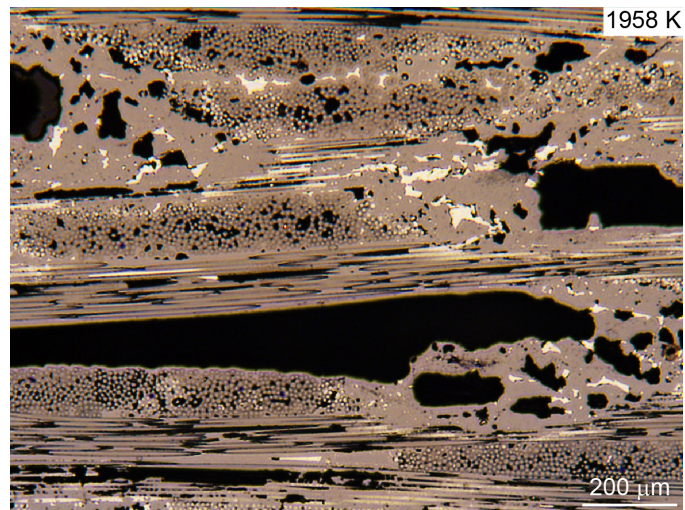

Figure 9.—High magnification optical micrograph of a preform melt-infiltrated with Cr-25%Si at 1958 K for 3600 s showing evidence of fiber fusion.
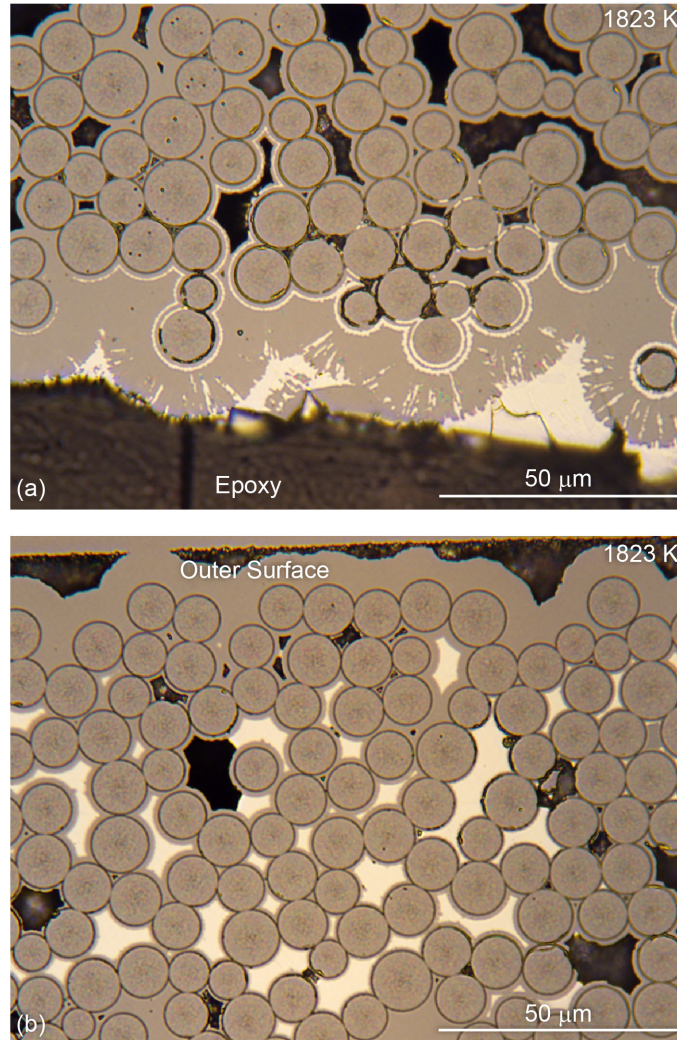
Figure 10.—Optical micrographs of a preform melt-infiltrated with
Cr-25%Si at 1823 K for 3600 s. (a) Double and single ring
microstructures consisting of solidified silicide regions around
the fibers, and silicide infiltration along the columnar grain
boundaries in the SiC coating in the outer region. (b) Absence
of the ring microstructures around the fibers and no evidence
of molten metal reaction with the coatings and fibers in the
inner region.

Figure 11 shows the plots of V_I and V_U against T_{MI}, where the error bars represent the 95% confidence limits. The vertical broken lines represent the solidus and liquidus absolute temperatures for Cr-25%Si [28]. The lower horizontal broken line represents the average value of V_0 in the as-received Tyranno SA3 preform measured by the immersion density method. The upper horizontal broken line is the average total void volume fraction, V_T, in the preform representing the average of the summation, $V_I + V_U$ measured by the microstructural technique. An examination of Figure 11 reveals that the measured values of V_I lie within a range $3.7\% \leq V_I \leq 11.9\%$ independent of T_{MI}. Several possible factors could limit the amount of molten material available to infiltrate the preforms. First, poor wettability of molten Cr-25%Si on the Tyranno SA3 fibers cannot be ruled out without conducting detailed studies on the wettability of Cr-25%Si on SiC substrates. Second, as noted earlier, the values of T_{MI} correspond to

the two-phase (β-Cr$_5$Si$_3$ + L) region except in the case when T$_{MI}$ = 1958 K. Therefore, it is possible that there was insufficient molten metal to fill the surface-connected voids in the specimens. This possibility is examined in Section 3.3. Third, as reported in an earlier study [27], the amount of (W$_{CS}$)$_{exp}$ lost due to the decomposition of the silicide in the vacuum environment of the MI furnace will increase with increasing values of T$_{MI}$. The possibility of weight loss due to the decomposition of Cr$_5$Si$_3$ in high vacuum at high temperatures is examined in Section 3.4.

3.3   Lever Rule Estimates of the Weight of the Molten Metal

As shown in Figure 11, since all the specimens except one were melt-infiltrated in the two-phase (β-Cr$_5$Si$_3$ + L) region (Figure 1), only the melted portion of the original charge can infiltrate the preform with the unmelted β-Cr$_5$Si$_3$ remaining on the outer surface of the specimen. Therefore, it is important to examine if (W$_{CS}$)$_{exp}$ was sufficient to produce enough molten alloy to theoretically fill the voids in the preform. To make these calculations, the silicon compositions at the solidus and liquidus lines corresponding to the values of T$_{MI}$ were estimated from the binary Cr-Si phase diagram in order to determine the relative wt.% of β-Cr$_5$Si$_3$ and L using the Lever rule (Figure 1) [28]. It is cautioned that only approximate values of the silicon compositions could be determined due to the fact that solidus line exhibits a steep upward curvature becoming almost parallel to the temperature axis above 1873 K. Figure 11(a) shows the calculated values of L(wt.%) plotted against T$_{MI}$. The amount of L gradually increases with increasing T$_{MI}$ until 1873 K before swinging upwards at a steeper slope. The maximum weight of the molten metal, (W$_{MI}$)$_{exp}$, available to infiltrate the preform was estimated using (W$_{MI}$)$_{exp}$ = W$_{CS}$)$_{exp}$*(L(wt.%)/100).

Figure 12(b) shows the variation of (W$_{MI}$)$_{exp}$ against T$_{MI}$ for 1778 K (T$_S$) $\leq$ T$_{MI}$ $\leq$ 1923 K. The values of (W$_{CS}$)$_{exp}$ varied between 2.2 and 12.5 g with the corresponding values of (W$_{MI}$)$_{exp}$ varying between 0.33 and 4.7 g, respectively. Noting that V$_0$ varied between 23.8 to 31.5% and using the density of 6.05 g/cm^3 for Cr-25%Si [35], the average amount of silicide required to fill all the open surface-connected voids in a 10 x 10 x 2.1 mm preform would be 0.3 to 0.4 g assuming θ_e = 0. For the smallest value of (W$_{CS}$)$_{exp}$ = 2.2 g used in the present investigation, the estimated value of (W$_{MI}$)$_{exp}$ was 0.33 g, which was close to the

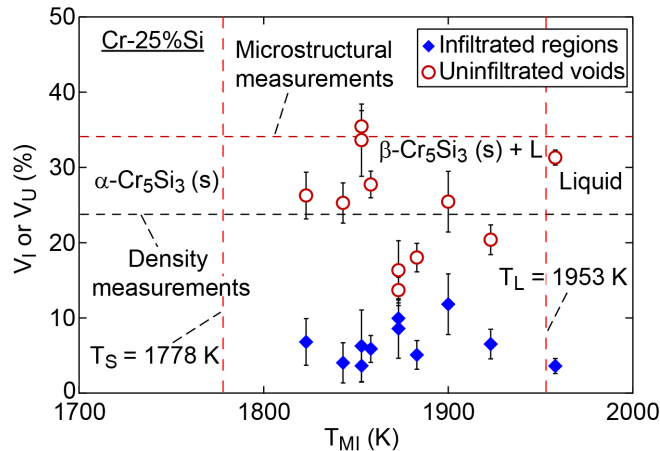Figure 11.—Plots of V$_I$ and V$_U$ against T$_{MI}$ showing that the volume fraction of melt-infiltrated voids were less than 12% and independent of T$_{MI}$ and t$_{MI}$. The vertical broken lines represent T$_S$ and T$_L$ for Cr-25%Si (Figure 1) [28]. The lower and upper horizontal broken lines represent V$_0$ and V$_T$ in the as-received preforms, respectively.
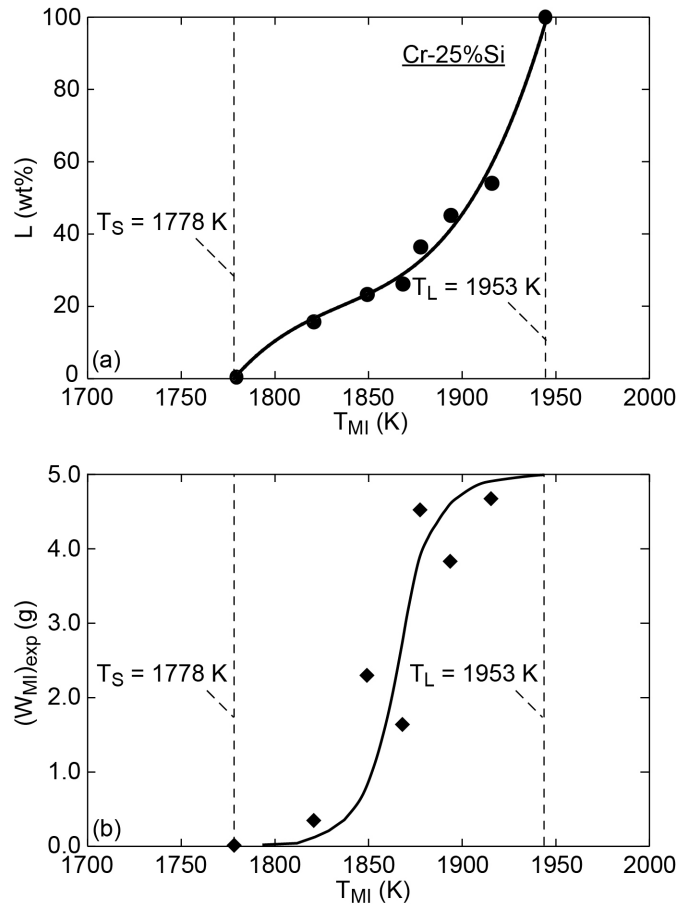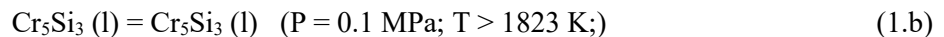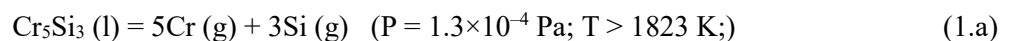
Figure 12.—Variation of (a) L (wt.%) and (b) $(W_{MI})_{exp}$ against T_{MI} for Cr-25%Si. The vertical broken lines represent T_S and T_L for Cr-25%Si [28].

average amount required to fill the open voids in the preforms. As shown in Figure 11(b), in all instances, the amount of Cr_5Si_3 charge used far exceeded $(W_{MI})_{exp}$ so that it can be concluded that in the absence of vaporization, there was sufficient molten metal available to infiltrate the preform in these experiments. The effect of material loss due to volatilization of the molten metal during MI of the preforms is discussed in Section 3.4.

3.4   Weight Loss Due to the Volatilization of Cr_5Si_3

As noted in an earlier paper on the MI of Tyranno SA3 preforms with $CrSi_2$, it was concluded that the decomposition of $CrSi_2$ in a vacuum environment was significant enough to lead to incomplete MI of the preform [27]. The decomposition of Cr_5Si_3 at high temperatures in a vacuum environment of 1.3×10^{-4} Pa $(1.0\times10^{-6}$ torr) is given by Equation (1.a) while Equation (1.b) suggests its stability at 0.1 MPa (1 atm.).

$$Cr_5Si_3 \text{ (l)} = 5Cr \text{ (g)} + 3Si \text{ (g)} \quad (P = 1.3\times10^{-4} \text{ Pa; } T > 1823 \text{ K;}) \tag{1.a}$$

$$Cr_5Si_3 \text{ (l)} = Cr_5Si_3 \text{ (l)} \quad (P = 0.1 \text{ MPa; } T > 1823 \text{ K;}) \tag{1.b}$$

Details of the computational thermodynamic analyses using the FactSage™[9] software confirmed the decomposition of Cr_5Si_3 at and above 1823 K under a vacuum of 1.3×10^{-4} Pa and its stability under a pressure of 0.1 MPa (1 atm.) (Table III)[10].

TABLE III.—PREDICTED FACTSAGE™ RESULTS SHOWING THE EQUILIBRIUM AMOUNTS OF THE STABLE PRODUCTS OR REACTANTS FOR SEVERAL REACTIONS OCCURRING AT 1823 K UNDER PRESSURES OF 1.3×10^{-4} Pa (1.0×10^{-6} torr) AND 10^5 Pa (1 atm.), RESPECTIVELY

Evaluated Reaction	P (Pa)	T (K)	Products	Equilibrium amount (mol)
Cr_5Si_3 (l) → 5 Cr(g) + 3 Si(g) (Eq. (1.a))	1.3×10^{-4}	1823	Cr(g) Si(g)	5.0 3.0
Cr_5Si_3 (l) → Cr_5Si_3 (l) (Eq. (1.b))	1.0×10^5	1823	Cr(g) Si(g) Cr_5Si_3(l)	0 0 1.0
BN(s) → B(s) + 1/2 N_2(g) (Eq. (3.a))	1.3×10^{-4}	1823	B(g) N_2(g)	1.0 5.0×10^{-1}
BN(s) → BN(s) (Eq. (3.b))	1.0×10^5	1823	B(g) N_2(g) BN(g) N(g) BN(s)	0 0 0 0 1.0
SiC(s) → Si(g)+ C(s) (Eq. (4.a))	1.3×10^{-4}	1823	Si(g) SiC_2(g) C(g) C3(g) Si_2C(g) C(s)	9.7×10^{-1} 2.3×10^{-2} 3.6×10^{-4} 3.1×10^{-4} 3.0×10^{-4} 9.5×10^{-1}
SiC(s) → SiC(s) (Eq. (4.b))	1.0×10^5	1823	Si(g) SiC_2(g) C(s) SiC(s)	0 0 0 1.0
Cr_5Si_3(l) + 2 C(s) → 5 Cr(g) + 3 Si(g) + 2 C(s) (Eq. (5.a))	1.3×10^{-4}	1823	Cr(g) Si(g) SiC_2(g) C(g) C_3(g) SiC_2(g) C(s)	5.0 2.9 0.07 2.9×10^{-3} 2.5×10^{-3} 3.3×10^{-4} 1.9
Cr_5Si_3(l) + 2 C(s) → 7/5 SiC(s) + 3/5 Cr_4C(s) + 1/2 Cr_5Si_3(l) (Eq. (5.b))	1.0×10^5	1823	SiC(s) Cr_4C(s) Cr_5Si_3(l)	1.4 0.59 0.53

---

[9] Trademark Thermfact and GTT-Technologies.
[10] Only the amounts of products predicted to be greater than 10^{-4} mol by the FactSage calculations are included in Table III.

The weight of molten metal that vaporized, W_V, and the remaining weight of the molten metal, W_R, were estimated from the empirical Equations (2.a) and (2.b) [27]

$$W_V = (W_{MI})_{exp} (t/\tau)^n \exp (-Q_v/RT_{MI}) \qquad (2.a)$$

$$W_R = (W_{MI})_{exp} - W_V = (W_{MI})_{exp} [1 - (t/\tau)^n \exp (-Q_v/RT_{MI})] \qquad (2.b)$$

where t is the transient time taken for the charge to attain the MI temperature after it melts[11], Q_v is the activation energy for volatilization, R is the universal gas constant, and n and τ are adjustable parameters[12]. The normalizing parameter τ ensures that t/τ is dimensionless, where $\tau > 0$. The experimental value Q_v/R of 3380 K for Cr_5Si_3 was used for evaluating W_V and W_R [36].

Figure 13(a) and (b) show the variations of W_V and W_R against T_{MI}, respectively, for values of $n = \frac{1}{5}, \frac{1}{4}$, and $\frac{1}{3}$ as depicted by the open symbols. The experimental values of $(W_{MI})_{exp}$ represented by the solid diamonds are included for comparison. A close examination of Figure 13(a) and (b) reveals that W_V and W_R are relatively insensitive of the magnitudes of n when $T_{MI} \leq 1873$ K in contrast to when $T_{MI} > 1873$ K. Importantly, it is evident that the choice of $n = \frac{1}{3}$ is unrealistic since it predicts $W_V > (W_{MI})_{exp}$ (Figure 13(a)). In comparison, the assumed values of $n = \frac{1}{5}$ and $\frac{1}{4}$ lead to more realistic predicted values of $W_V < (W_{MI})_{exp}$ and $W_R > 0$. It is noted that the values of W_R for $n = \frac{1}{4}$ are independent of T_{MI} (Figure 13(b)) consistent with the observations that V_I is independent of T_{MI} (Figure 11). Although W_R was slightly more than 0.3 to 0.4 g required to completely fill the open voids, it is important to note this is only a theoretical possibility when $\theta_e = 0°$ for complete wettability with no blockage of the surface-connected voids due to solidified metal. In reality, the fact that $\theta_e \sim 40°$ for Cr_5Si_3 [29], a low value of γ_{SV}, and the possibility that the surface-connected voids could be choked off from the surface due to solidified alloy is likely to lead to incomplete infiltration of the preforms. The values of W_R vary between about 0.7 and 1.8 g for $n = \frac{1}{5}$ (Figure 13(b)).

3.5 Ring Microstructures

As discussed in Section 3.2, single or double ring microstructures were observed primarily near the outer surfaces of the preform below the CVI SiC coating (Figure 10(a)). These microstructures were uncommon but not completely absent in the interior regions of the preform (Figure 10(b)). Figure 14(a) demonstrates the microstructural differences between the outer surface of an infiltrated preform and its interior regions. At the interface between the CVI SiC coating and the molten Cr-25%Si, the microstructure shows clear evidence of a reaction and possible re-precipitation of SiC particles (e.g., gray particles in the dotted circled region). Not surprisingly, the molten metal had penetrated along the columnar grain boundaries in the SiC coating (Figure 10(a)). A close examination of the boxed region in Figure 14(a) at high magnifications revealed that the BN coating was absent (Figure 14(b)). For example, the BN coatings around fibers A and B are either completely or partially absent, respectively. It is evident that the molten metal has filled the voids left around many of these fibers with the missing BN coating (Figure 10(a) and Figure 14(b)). The outer rings were commonly observed either at the boundaries of the CVI SiC with the coating material or at the boundaries of CVI SiC coatings around adjacent fibers (Figure 14(b)). Although the boundaries between the solidified metal and the CVI SiC or the fibers often looked jagged, a close examination of the microstructure did not show evidence of a reaction (Figure 14(b)). Similarly, the reaction between the molten metal and the CVI SiC was absent in the interior of the preform consistent with the microstructural observations of the outer rings (Figure 10(b) and Figure 14(a)).

---

[11] Note: t is different from t_{MI}. At a heating rate of 600 K/h, t varied between 270 and 870 s to attain T_{MI}.
[12] In an earlier paper, it was implicitly assumed that the constant $\tau = 1$ s [27].
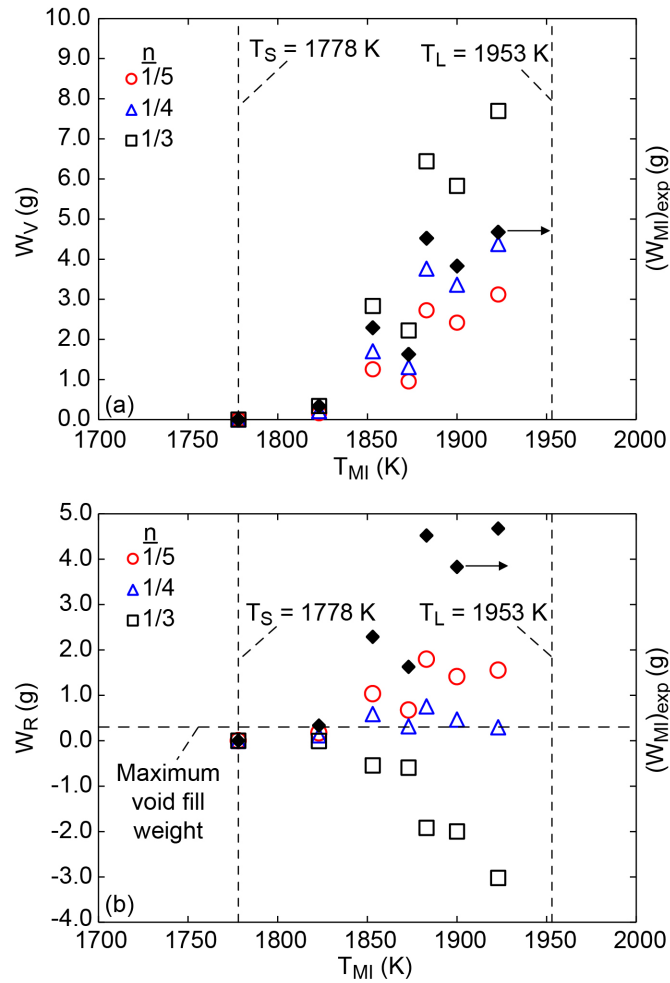
Figure 13.—Variations of (a) W_V and (b) W_R against T_{MI} for values of n = 1/5, 1/4, and 1/3 as depicted by the open circle, triangle and square symbols, respectively. Variation of $(W_{MI})_{exp}$ and T_{MI} represented by the solid diamond symbols are shown for comparison in both plots. The vertical broken lines represent T_S and T_L for Cr-25%Si [28]. The horizontal broken line in (b) is the maximum weight of charge required to fill all the open voids in the preforms.

Figure 14.—(a) Low magnification SE micrograph of a preform melt-infiltrated with Cr-25%Si at 1823 K for 3600 s showing double and single ring microstructures around the outer fibers but not around the interior fibers. The molten silicide has infiltrated the columnar grain boundaries of the CVI SiC coating with remnant SiC particles observed in the Cr-25%Si layer. The gray particles encircled by the dotted circle indicate probable re-precipitated SiC. (b) High magnification BSE image of the boxed regions shown in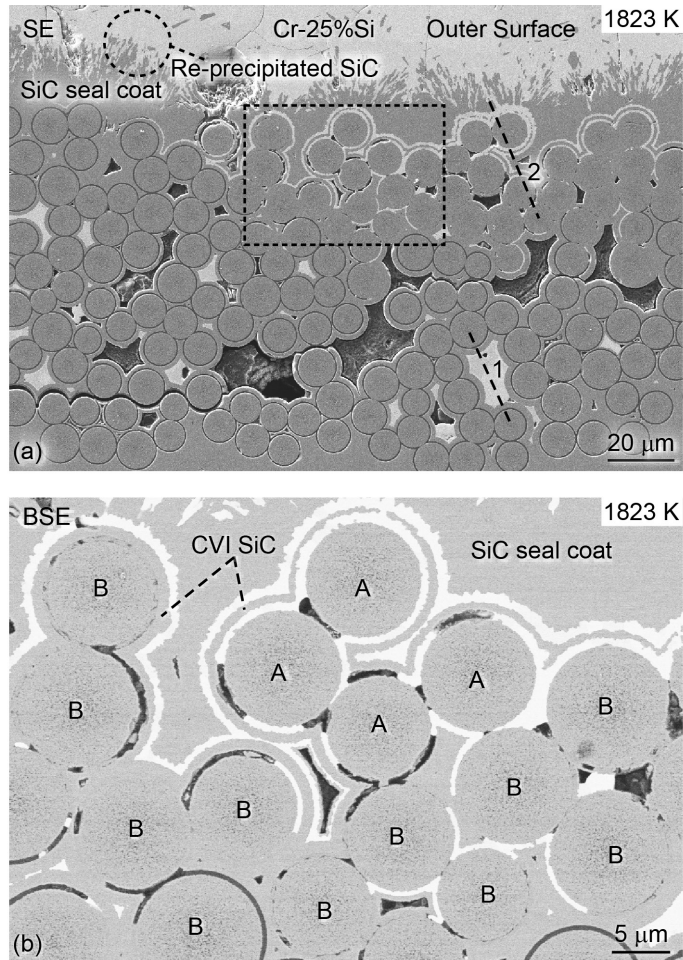 (a) showing that the voids left around fibers A and B after BN and CVI SiC coating volatilization are partially or completely filled with the silicide.

The fact that the molten metal did not react with the CVI SiC material in the interior of the preform does not necessarily indicate that there would be no reaction after long periods of time at high temperature exceeding t_{MI}. Figure 15 demonstrates that the molten metal attack is severe close the outer surface of the preform compared to the interior. Interestingly, several fibers show evidence of molten silicide encroachment starting from their centers and spreading outwards towards the periphery until the fibers are destroyed. In contrast, other neighboring fibers do not show any infiltration at their centers even those with solidified metal rings around them.
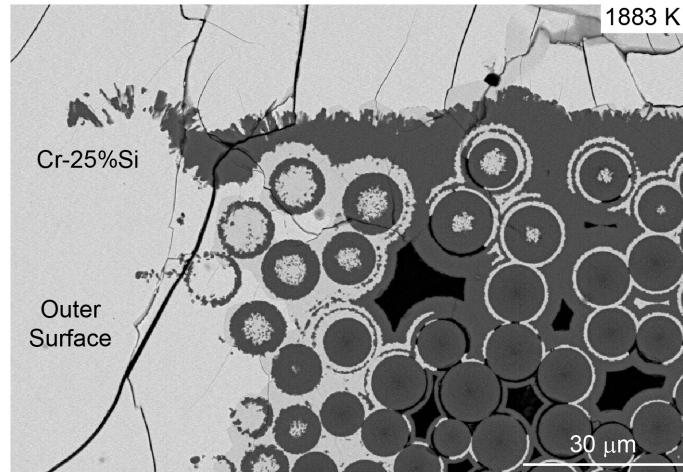
Figure 15.—High magnification BSE image of a preform melt-
infiltrated with Cr-25%Si at 1883 K for 3600 s showing the
almost complete destruction of some of the outer fibers and
remnants of the CVI SiC coating.

Precise sections were milled along lines 1 and 2 by FIB parallel to the orientation of the fibers in order to get a depth perception of the microstructural differences in the fibers located at the periphery and interior of the preforms (Figure 14(a)). Figure 16(a) and (b) show the microstructural features along lines 1 and 2, respectively. A close examination of Figure 16(a) corresponding to the preform interior region reveals that the BN and CVI SiC coatings are intact and the SiC_f fibers show some discontinuous porosity. The molten Cr-25%Si has filled the gap between the CVI SiC regions as shown in Figure 14(a). There is no evidence of molten metal attack in the upper regions of milled section[13]. In contrast, observations of the milled section from line 2 near the periphery of the preform in Figure 14(a) shows clear evidence of missing BN coating around the fibers, where the empty channels were often filled with silicide (Figure 16(b) and (c)). Figure 16(c) is high magnification view of the right hand section of Figure 16(b). Interestingly, the SiC_f fibers showed an extensive porous network (Figure 16(c)) unlike the relatively dense fibers observed in Figure 16(a), which would enable the molten silicide to infiltrate them (Figure 15). The microstructures revealed that the molten metal had infiltrated the CVI SiC regions of the specimen (Figure 16(b) and (c)). A careful examination of the microstructures revealed that the molten metal had primarily infiltrated the CVI SiC regions through a porous interconnected network thereby producing a macroscopic, uneven, jagged liquid-solid front with isolated pockets of solidified metal at some distance from the interface (Figure 16(b)). The subsequent rupture and collapse of the struts forming the porous network under the mechanical force exerted on them by the advancing molten metal would result in the interconnection and overlap of the neighboring filled pores resulting in the observed blob of solidified alloy seen in the fibers and in the CVI SiC.

---

[13] The white regions at the bottom rear section of the micrograph are most likely projections of the neighboring milled regions of the preform in the field of view and do not represent an unambiguous evidence of molten metal attack.
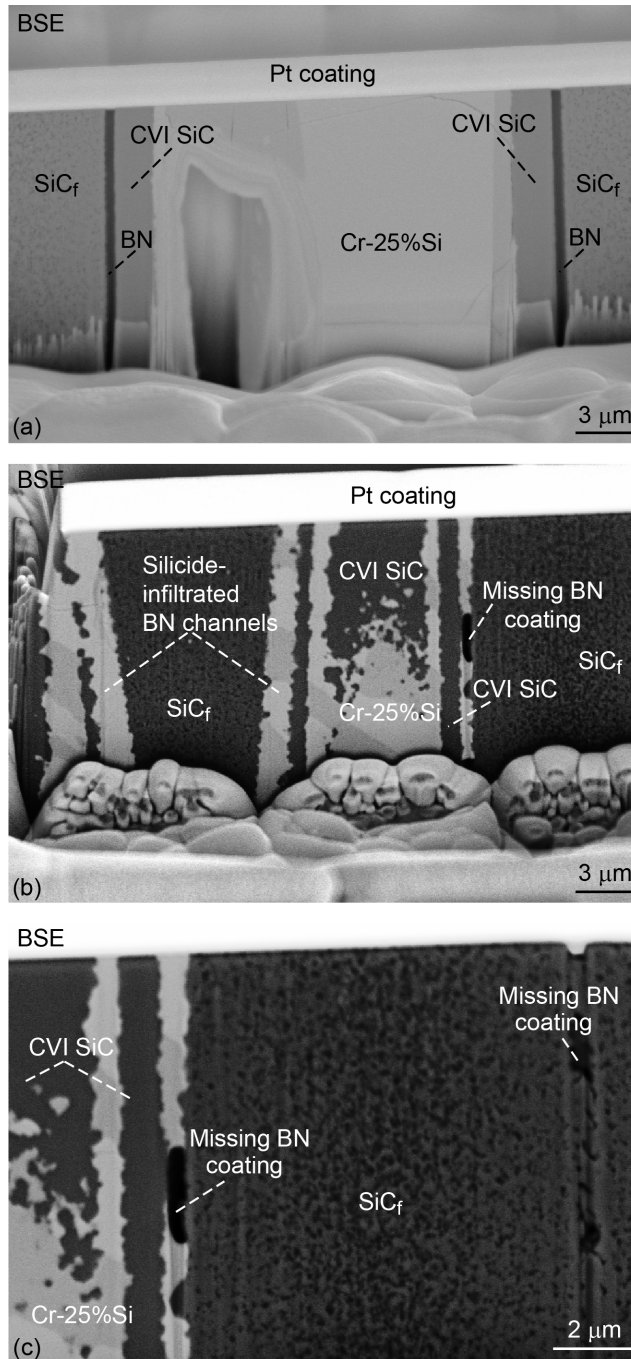
Figure 16.—(a) Back scattered electron micrograph of a FIB-milled section parallel to the fiber orientations along line 1 in Figure 14(a) showing that the BN and the CVI SiC coatings are intact while the SiC_f fibers show some discontinuous porosity. The voids between adjacent CVI SiC coatings are partially filled with Cr-25%Si with no evidence of molten metal attack of the BN and the CVI SiC coatings, and the SiC_f fibers. (b) Low and (c) high magnification BSE images of a FIB-milled section parallel to the fiber orientations along line 2 in Figure 14(a). The silicide has infiltrated the voids in the regions where the BN and the CVI SiC coatings were missing. The SiC_f fibers show a network of porosity without silicide infiltration.

Since the BN coatings on the outer fibers were missing and the SiC_f showed an extensive network of porosity (Figure 16(b) and (c)), it stands to reason that BN and SiC may have volatilized at high temperatures in the high vacuum melting furnace. To examine this possibility, FactSage thermodynamic calculations were conducted to investigate the thermal stability of BN (s) and SiC (s) as well as the probability that molten Cr_5Si_3 (l) will be reduced by carbon at 1823 K. The calculations were conducted for a vacuum of 1.3×10^{-4} Pa (1.0×10^{-6} torr) and compared with results for a high pressure of 0.1 MPa (1 atm.) to determine the thermal stability of the coatings. Table III shows the predicted products for amounts above 10^{-4} mol for the reactants given by Equations (3.a) to (5.a), where the equations include only products with predicted amounts greater than 0.5 mol.

$$BN\ (s) \rightarrow B\ (g) + \frac{1}{2}\,N_2\ (g) \qquad\qquad (1.3 \times 10^{-4}\ \text{Pa}; T > 1823\ \text{K}) \qquad (3.a)$$

$$BN\ (s) \rightarrow BN\ (s) \qquad\qquad (0.1\ \text{MPa}; T > 1823\ \text{K}) \qquad (3.b)$$

$$SiC\ (s) \rightarrow Si\ (g) + C\ (s) \qquad\qquad (1.3 \times 10^{-4}\ \text{Pa}; T > 1823\ \text{K}) \qquad (4.a)$$

$$SiC\ (s) \rightarrow SiC\ (s) \qquad\qquad (0.1\ \text{MPa}; T > 1823\ \text{K}) \qquad (4.b)$$

$$Cr_5Si_3(l) + 2\,C(s) \rightarrow 5\,Cr(g) + 3\,Si(g) + 2\,C\ (s) \qquad (1.3 \times 10^{-4}\ \text{Pa}; T > 1823\ \text{K}) \qquad (5.a)$$

$$Cr_5Si_3(l) + 2\,C(s) \rightarrow \frac{7}{5}\,SiC(s) + \frac{3}{5}\,Cr_4C(s) + \frac{1}{2}\,Cr_5Si_3(s) \qquad (0.1\ \text{MPa}; T > 1823\ \text{K}) \qquad (5.b)$$
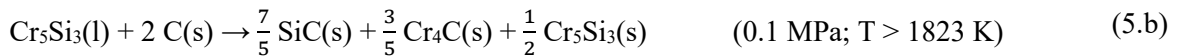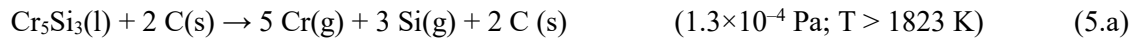
Equations (3.a), (3.b), to (5.a) predict the formation of gaseous B (g), Cr (g), N_2 (g) Si (g), and C (s) as major reactant products under the MI processing conditions used in the present investigation. In contrast, when MI is conducted under 0.1 MPa, Equations (3.b) and (4.b) suggest that the BN and CVI SiC coatings are likely to be stable. Interestingly, Equation (5.a) indicates that the molten Cr_5Si_3 is unlikely to react with carbon under a vacuum of 1.3×10^{-4} Pa (1.0×10^{-6} torr) owing to the possible volatilization of the silicide, whereas Equation (5.b) suggests that carbon will react with the molten silicide to form SiC (s) and Cr_4C (s) under a 0.1 MPa external pressure.

It is likely that the SiC particles within the Cr-25%Si layer as denoted by the circled region in Figure 14(a) are re-precipitated SiC. However, the thermal stability of these re-precipitated SiC particles and coatings under high vacuum and high MI temperatures is likely to be low, and given enough time, it is expected that they would eventually decompose in accordance with Equation (4.a). As noted earlier, the decomposition of BN and CVI SiC coatings in the outer regions of the preforms would leave voids, which would fill-up with molten metal to form the observed ring microstructures.

Importantly, the FactSage calculations revealed that BN, Cr-25%Si and SiC are stable and would not decompose under these conditions (Table III). Thus, the general absence of the molten silicide ring microstructure in the interior regions of the specimens (Figure 10(b) and Figure 16(a)) suggests that there was probably sufficient positive pressure in the interior to ensure that BN, Cr-25%Si and SiC were stable during MI. However, it is expected that these compounds would eventually decompose at high temperatures under a dynamic vacuum when $t_{MI} \gg 3600$ s thereby resulting in the formation of ring microstructures in the interior regions of the specimens.

4.0   Summary and Conclusions

Melt infiltration studies of woven preforms of 2D Tyranno SA3 fibers with Cr-25%Si were conducted between 1823 and 1958 K under a vacuum varying between 1.3×10^{-2} and 6.7×10^{-4} Pa (10^{-4} and 5×10^{-6} torr) for infiltration times between 1800 and 3600 s. These values of T_{MI} corresponded mainly to the two-

phase β-Cr_5Si_3+liquid region of the Cr-Si binary phase diagram [28]. Careful microstructural observations revealed that less than 12% of the open void volume fraction had been infiltrated independent of the values of T_{MI} and t_{MI} even when a significant amount of solidified alloy was observed on the outer surfaces of the preforms for $T_{MI} \leq 1873$ K. In contrast, there was little or no solidified metal on the surfaces of most of the preforms for $T_{MI} > 1873$ K. Significant fiber deformation, fusion and shrinkage occurred for $T_{MI} > 1883$ K thereby suggesting an upper useful limit for T_{MI}. It was demonstrated using the Lever rule that the amount of charge was enough to produce sufficient molten metal to fill all the surface-connected voids in the preforms. The inability to completely fill the surface-connected voids between the fiber tows was attributed to the volatilization of the Cr-25%Si alloy based on FactSage thermodynamic calculations although the role of poor wettability could not be ruled out in the absence of experimental γ_{SV} and θ_e data.

Single and double ring microstructures were observed mainly near the outer regions of the preforms, where the molten metal had infiltrated and solidified in the regions previously occupied by the BN coating and at the boundaries between the CVI SiC coatings. In addition, high magnification BSE microstructural observations revealed the presence of a porous network in the SiC_f fibers, which were potential conduits for molten metal flow during MI. These observations also revealed that the molten silicide had infiltrated the CVI SiC coatings presumably through a fine porous network. The ring microstructures were not commonly observed in the interior regions of the preforms. FactSage thermodynamic calculations predicted that the BN and CVI SiC coatings would volatilize at high temperatures under the vacuum conditions used in the present investigation. However, they were predicted to be stable at high temperatures under a 0.1 MPa pressure. There was no unambiguous evidence that Cr-25%Si had reacted with either the BN or CVI SiC coatings during MI as evidenced by the microstructures present in interior regions of the infiltrated specimens. It was rationalized that the molten silicide had filled the voids left behind after the BN and CVI SiC coatings had volatilized during heat-up above the solidus temperature in the vacuum furnace thereby leading to the occurrence of ring microstructures primarily in the exterior regions of the preforms. Thus, it is suggested that MI of Tyranno SA3, and possibly other SiC_f preforms, with the Cr-25%Si alloy is best performed under a positive pressure sufficiently large enough to prevent the decomposition of the Cr-25%Si alloy and the BN and CVI SiC coatings. Additionally, T_{MI} should be less than 1883 K to prevent fiber fusion and damage. Finally, FactSage thermodynamic calculations indicate that molten Cr_5Si_3 would react with carbon at 1823 K and 0.1 MPa pressure to form SiC and Cr_4C.

References

1. D. Brewer, HSR/EPM Combustor Materials Development Program, *Mater. Sci. Eng. A.*, 1999, **A261**, p 284-291. https://doi.org/10.1016/S0921-5093(98)01079-X
2. H. Ohnabe, S. Masaki, K. M. Onozuka, K. Miyahara and T. Sasa, Potential Application of Ceramic Matrix Composites to Aero-Engine Components, *Composites: Part A.*, 1999, **30**, p 489-496. https://doi.org/10.1016/S1359-835X(98)00139-0
3. C. M. Grondahl and T. Tsuchiya, Performance Benefit Assessment of Ceramic Components in a MS9001FA Gas Turbine, *J. Eng. Gas Turbine Power*, 2000, 123, p 513-519. https://doi.org/10.1115/1.1335476
4. T. Kameda, Y. Itoh, T. Hishata and T. Okamura, Development of Continuous Fiber Reinforced Reaction Sintered Silicon Carbide Matrix Composite for Gas Turbine Hot Parts Application, *ASME*, 2000, Paper No. 2000-GT-67. https://doi.org/10.1115/2000-GT-0067

5.   R. J. Miller, Design Approaches for High Temperature Composite Aeroengine Components, *Comprehensive Composite Materials* (A. Kelly and C. Zweben eds.), 2000; **Vol. 6,** p 181-207. https://doi.org/10.1016/B0-08-042993-9/00138-8

6.   K. K. Chawla, *Ceramic Matrix Composites (2nd ed.)*, Kluwer Academic Publishers, Norwell, MA, 2003.

7.   R. Naslain, Design, Preparation and Properties of Non-Oxide CMCs for Applications in Engines and Nuclear Reactor: An Overview, *Comp. Sci. and Tech.*, 2004, **64**, p 155-170.

8.   G. S. Corman and K. L. Luthra, Silicon Melt Infiltrated Ceramic Composites (HiPerComp), *Handbook of Ceramic Composites* (N. P. Bansal ed.), Kluwer Academic Publishers, Boston, MA, 2005, p 99-115. https://doi.org/10.1007/b104068

9.   J. A. DiCarlo, H. M. Yun, G. N. Morscher and R. T. Bhatt, SiC/SiC Composites for 1200 ºC and Above, *Handbook of Ceramics, Glasses and Composites* (N. P. Bansal ed.), Kluwer Academic Publishers, Boston, MA, 2005, p 77-98. https://doi.org/10.1007/b104068

10.   J. A. DiCarlo and M. van Roode, Ceramic Composite Development for Gas Turbine Hot Section Components, *Proc. GT2006 ASME Turbo Expo 2006: Power for Land, Sea and Air*, Barcelona, Spain, ASME, 2006, Paper No. GT 2006-90151, p 221-231. https://doi.org/10.1115/GT2006-90151

11.   F. Christin, CMC Materials for Space and Aeronautical Applications, *Ceramic Matrix Composites* (W. Krenkel ed.), Wiley-VCH Verlag, 2008, p 327-351.

12.   M. C. Halbig, M. H. Jaskowiak, J. D. Kiser and D. Zhu, Evaluation of Ceramic Matrix Composite Technology for Aircraft Turbine Engine Applications, *Proceedings of the 51st AIAA Aerospace Sciences Meeting*, Grapevine, Texas, January 7-10, 2013, Paper No. AIAA-2013-0539, 2013. https://arc.aiaa.org/doi/pdf/10.2514/6.2013-539

13.   https://www.researchandmarkets.com/research/m3pjzn/global_ceramic, July 2017.

14.   F. W. Zok , Ceramic-Matrix Composites Enable Revolutionary Gains in Turbine Engine Efficiency, *Am. Ceram. Soc. Bull.,* 2016, **95**, p 22-28.

15.   G. N. Morscher, Stress-Dependent Matrix Cracking in 2D Woven SiC-Fiber Reinforced Melt-Infiltrated SiC Matrix Composites, *Comp. Sci. Tech.*, 2004, **64**, p 311-319.

16.   G. N. Morscher, M. Singh, J. D. Kiser, M. Freedman and R. Bhatt, Modeling Stress-Dependent Matrix Cracking and Stress-Strain Behavior in 2D Woven SiC Fiber Reinforced CVI SiC Composites. *Comp. Sci.. Tech.*, 2007, **67**, p 1009-1017.

17.   G. N. Morscher and V. V. Pujar, Design Guidelines for In-Plane Mechanical Properties of SiC Fiber-Reinforced Melt-Infiltrated SiC Composites, *Intern. J. Appl. Ceram. Techno.*, 2009, **6**, p 151-63.

18.   G. N. Morscher, Advanced Woven SiC/SiC Composites for High Temperature Applications, *Composites at Lake Louise conference*, Oct. 28-Nov. 2, 2007, Alberta, Canada. https://ntrs.nasa.gov/archive/nasa/ casi.ntrs.nasa.gov/20080006057.pdf.

19.   J. Steibel , G. S. Corman, R. C. Schikner and A. Szweda, Article and Method for Making Complex Shaped Preform and Silicon Carbide Composite by Melt Infiltration, U.S. Patent 6,258,737 B1, July 10, 2001.

20.   S. V. Raj, Thermal Expansion of Hot-Pressed Engineered Ceramic Materials, *Ceram Intern.* 2016, **42**, p 2557-69. https://doi.org/10.1016/j.ceramint.2015.10.058

21.   S. V. Raj, High Temperature Creep and Oxidation Resistant Chromium Silicide Matrix Alloy Containing Molybdenum, U. S. Patent No. 5,330,590 issued July 19, 1994.

22.   S. V. Raj, A Preliminary Assessment of the Properties of a Chromium Silicide Alloy for Aerospace Applications, *Mater. Sci. Eng. A.,* 1995, **192-193**, p 583-589.

23.   S, V. Raj, An Evaluation of the Properties of Cr_3Si Alloyed with Mo, *Mater. Sci. Eng. A.*, 1995, **201**, p 229-241.

24. R. M. Dickerson, S. V. Raj and I. E. Locci, A Preliminary Investigation of the Cr_3Si -Mo Pseudo-Binary Phase Diagram, *Proc. Mater. Res. Soc.*, Pittsburgh, PA., 1995, **vol. 364**, p. 949-954.

25. S. V. Raj, J. D. Whittenberger, B. Zeumer and G. Sauthoff, Elevated Temperature Deformation of Cr_3Si Alloyed with Mo, *Intermetall.*, 1999, **7**, p 743-755.

26. S. V. Raj, Development and Characterization of Hot-Pressed Matrices for Engineered Ceramic Matrix Composites (E-CMCs), *Ceram. Intern.*, 2019, **45**, p 3608-3619. https://doi.org/10.1016/j.ceramint.2018.11.021

27. S. V. Raj, Melt Infiltration Studies of 2D Tyranno SA3 Ceramic Matrix Composite Preforms with $CrSi_2$ Intermetallic Alloy, J. Am. Ceram. Soc., 2021, **104**, p 2966-2980.

28. A. B. Gokhale, G. J. Abbaschian, *Binary Alloy Phase Diagrams* (T. B. Massalski, H. Okamoto, P. R. Subramanian and L. Kacprzak eds.), 1990, **Vol. 2**, p 1333-1335.

29. J. A. Champion, B. J. Keene and S. Allen, Wetting of Refractory Materials by Molten Metallides, J. Mater. Sci. 1973, **8**, p 423-426.

30. M. L. Santella and A. J. Moorhead, A Review of Oxide, Silicon Nitride, and Silicon Carbide Brazing, *Annual North American Welding Research Seminar*, Columbus, OH, USA, 29 Sep.-Oct. 1, 1987, Report No. CONF-870981-1, Oak Ridge National Laboratory, Knoxville, TN, 1987. https://www.osti.gov/servlets/purl/6185784.

31. B. Drevet and N. Eustathopoulos, Wetting of Ceramics by Molten Silicon and Silicon Alloys: A Review, *J. Mater. Sci.*, 2012, **47**, p 8247-8260.

32. O. Dezellus and N. Eustathopoulos, Fundamental Issues of Reactive Wetting by Liquid Metals, *J. Mater. Sci.*, 2010, **45**, p 4256-4264.

33. G. W. Liu, M. L. Muolo, F. Valenza and A. Passerone, Survey on Wetting of SiC by Molten Metals, *Ceram. Intern.*, 2010, **36**, p 1177-1188.

34. R. Warren and C. H. Andersson, Silicon Carbide Fibres and their Potential for Use in Composite Materials Part II, *Composites*, 1984, **15**, p 101-111.

35. https://materialsproject.org/materials/mp-7506/

36. C. E. Myers, G. A. Murray, R. J. Kematick and M. A. Frisch, *Vaporization Thermodynamics of Chromium Silicides*, Report ADR-A162-286, Office of Naval Research, Arlington, VA, 1985.